Filter-Probe Diffusion Imaging Improves Spinal Cord Injury Outcome Prediction

Nathan P. Skinner, PhD[1,2], **Seung-Yi Lee**[1,3,4], **Shekar N. Kurpad, MD, PhD**[1], **Brian D. Schmit, PhD**[5], **L. Tugan Muftuler, PhD**[1], and **Matthew D. Budde, PhD**[1]

[1]Department of Neurosurgery, Medical College of Wisconsin, Milwaukee, WI

[2]Medical Scientist Training Program, Medical College of Wisconsin, Milwaukee, WI

[3]Neuroscience Doctoral Program, Medical College of Wisconsin, Milwaukee, WI

[4]Biophysics Graduate Program, Medical College of Wisconsin, Milwaukee, WI

[5]Department of Biomedical Engineering, Marquette University, Milwaukee, WI

Abstract

Objective—Diffusion weighted imaging (DWI) is a powerful tool for investigating spinal cord injury (SCI), but has limited specificity for axonal damage- the most predictive feature of long-term functional outcome. In this study, a technique designed to detect acute axonal injury, filter-probe double diffusion encoding (FP-DDE) is compared with standard DWI for predicting long-term functional and cellular outcomes.

Methods—This study extends FP-DDE to predict long-term functional and histological outcomes in a rat SCI model of varying severities(n=58). Using a 9.4T MR system, a whole-cord FP-DDE spectroscopic voxel was acquired in three minutes at the lesion site and compared to DWI at 48 hours post-injury. Relationships with chronic (30-day) locomotor and histological outcomes were evaluated with linear regression.

Results—The FP-DDE measure of parallel diffusivity ($ADC_\parallel$) was significantly related to chronic hind limb locomotor functional outcome (R^2=0.63, p<0.0001) and combining this measurement with acute functional scores demonstrated prognostic benefit versus functional testing alone (p=0.0007). Acute $ADC_\parallel$ measurements were also more closely related to the number of injured axons measured 30 days after the injury than standard DWI. Furthermore, acute FP-DDE images showed a clear and easily interpretable pattern of injury that closely corresponded chronic MRI and histology observations.

Interpretation—Collectively, these results demonstrate FP-DDE benefits from greater specificity for acute axonal damage in predicting functional and histological outcomes with rapid acquisition

and fully automated analysis, improving over standard DWI. FP-DDE is a promising technique compatible with clinical settings with potential research and clinical applications for evaluation of spinal cord pathology.

Keywords

Introduction

Early identification of spinal cord injury (SCI) severity can affect long-term outcome by affecting early clinical decision-making[1] while providing important information to patients[2]. Thus, several strategies have been devised to provide early and accurate prognostication of injury severity. Current clinical standards rely on functional testing, such as ASIA scoring for characterizing injury[3], but are often unreliable for predicting long-term functional outcomes due to changes in score over time within some patients[4]. Clinical magnetic resonance imaging (MRI), such as T_2-weighted imaging, has aided SCI assessment, but similarly does not reliably predict long-term functional outcomes due to the lack of specificity to axonal damage[5–7], the strongest pathological correlate of long-term functional outcome following SCI[8, 9]. Thus, techniques such as diffusion weighted imaging (DWI), and diffusion tensor imaging (DTI)[10, 11] in particular, have garnered considerable interest as noninvasive biomarkers of SCI due to their sensitivity to microscopic axonal damage[12, 13].

DTI in experimental SCI[14] has shown decreased diffusion in white matter fiber tracts related to axonal damage[15–17], but its use in acute human SCI is limited by technical hurdles of spinal cord imaging, particularly in the acute care setting, as well as the heterogeneity of human SCI. Moreover, despite sensitivity to injury[18], it cannot disambiguate the effects of axonal damage from confounding changes from edema and inflammation accompanying injury[19]. One approach to disentangle these effects uses mathematical models to separate axonal signal from edema and inflammation, with a variety of proposed solutions[20–25]. Of these, the White Matter Tract Integrity (WMTI) model showed the greatest ability to disambiguate axonal and extracellular water in a simulation study[19]. However, these techniques require longer acquisitions times, considerable post-processing, and added complexity that limit their clinical feasibility and ease of use for acute SCI.

An alternative approach has been recently demonstrated to achieve similar disambiguation during the acquisition stage as opposed to the post-processing stage. Instead of using diffusing weighting solely to measure diffusion properties of tissues, diffusion weighting can also serve as a filter to suppress undesirable features in the tissue. This technique, known as filter-probe double diffusion encoding (FP-DDE), previously showed improved specificity to axonal damage over DTI and WMTI in simulations[19] and reflected the severity of injury in the acute stage using a rat model of contusion SCI[26]. Furthermore, recent advances have improved the potential clinical use of DDE imaging on clinical hardware[27]. However, clinical translation and utility also requires insight into the relationship between FP-DDE and long-term function, and it is hypothesized that the improved specificity for axonal damage with the diffusion filter will enable better prediction of functional outcomes

compared with traditional DTI and WMTI measures. In this study, we applied a fast and objective measurement from FP-DDE to prognosticate locomotor outcomes in the rodent model in comparison with DTI and WMTI. Furthermore, the relationship between FP-DDE and the underlying tissue structure was evaluated using quantitative histology. The filter-probe technique was also implemented using a traditional imaging readout as a demonstration of its flexibility for individual applications. In total, these studies provide important validation of the filter-probe technique for prognostic purposes in clinical applications.

Methods

Animals and Spinal Cord Injury Procedure

All animal procedures were approved by the Institutional Animal Care and Use Committees (IACUC) at the Medical College of Wisconsin (MCW), Clement J. Zablocki VA Medical Center, and Northwestern University (NU). Experiments were conducted at two separate sites chronologically due extended downtime of the MRI system at the Medical College of Wisconsin. All experimental procedures were performed in their entirety at each of the respective institutions. A total of 58 female Sprague-Dawley rats (250–275 g; Charles River) were used in this study at both sites (MCW n=23, NU n=35) with all experiments performed by the same personnel.

For the injury procedure, rats were anesthetized with 4% inhaled isoflurane, ensuring absence of leg flexion-withdrawal and corneal reflexes. The back was shaved and sterilized with povidone-iodine, and an incision was made over the mid-thoracic region. A laminectomy was performed on the T10 spinal segment, the animal was positioned in a MASCIS impactor (W.M. Keck Center for Collaborative Neuroscience; Piscataway, NJ), and a 10 g rod was dropped from a height of 0, 10, 25, or 50 mm to induce a sham (MCW n=6, NU n=7), mild (MCW n=5, NU n=8), moderate (MCW n=5, NU n=8), or severe (MCW n=7, NU n=10) injury, respectively. After surgery, rats were placed on postoperative care, including twice-daily bladder expression, one dose of enrofloxacin (10 mg/kg subcutaneously; Bayer Healthcare LLC; Shawnee Mission, KS), buprenorphine hydrochloride (0.1–0.5 mg/kg subcutaneously; Rickitt Benckiser Health Care Ltd; Hull, UK), and 6 cc of lactated Ringer's solution. Animals were kept under postoperative care procedures until bladder function returned and no signs of infection or stress were evident.

Magnetic Resonance Imaging

In vivo magnetic resonance experiments were performed on two separate Bruker 9.4 T Biospec Systems, MCW (Site 1) and NU (Site 2), with different software versions, Paravision 5.1 and 6.0.1, respectively, but with nearly all other features similar, including identical radiofrequency coils and magnetic field gradient performance. A commercial 4-channel surface coil array (Bruker Biospin) was used for signal reception and a 72 mm diameter quadrature volume coil was used for transmission.

Animals were placed supine with the T10 spinal level centered over the receiver coil array and secured to a custom-made cradle to minimize motion. MRI procedures were performed

on injured animals at 2 days (acute) and 30 days (chronic) post-injury. A sagittal FLASH gradient echo image was used as a reference to position slices at the T10 lesion epicenter. For DTI data, conventional pulsed gradient spin echo (PGSE) acquisitions employed a diffusion weighted spin-echo echo planar imaging (DW-EPI) sequence as described previously[26]. Briefly, a 4-shot, respiratory-gated EPI acquisition (TE=28 ms; TR 1500 ms, varied by respiratory rate) was used to collect 12 slices centered on the injury epicenter with an in-plane resolution of 0.20×0.20 mm^2, slice thickness of 1.0 mm, and 0.5 mm slice gap. A total of four signal averages were used to acquire 30 unique diffusion directions[28] with b-values of 500, 1000, and 2000 s/mm^2 using 7 ms gradient duration (δ) and 13.4 ms gradient separation ( ) and 15 non-diffusion-weighted images. This full DW-EPI acquisition required approximately 65 minutes of imaging time.

FP-DDE implementation used a twice-refocused spin echo sequence modified to include two pairs of Stejskal-Tanner diffusion weighting gradients surrounding each of the refocusing radiofrequency pulses as described previously[26]. FP-DDE diffusion encoding consisted of an initial diffusion weighting "filter" applied perpendicular to the spinal cord axis with a non-varying strength b=2000 s/mm^2. This was followed by a second diffusion weighting "probe" gradient pair applied parallel to the spinal cord axis using nine separate b-values ranging from 0–2000 s/mm^2. For a whole-cord diffusivity measure, FP-DDE encoding was coupled with a Point-RESolved Spectroscopy (PRESS) readout using a single voxel ($10 \times 10 \times 6$ mm^3) centered on the T10 lesion epicenter. Gradient timings included δ=6 ms and =12 ms. Voxel shimming was performed using the Bruker MAPSHIM for first-order and Z^2 shims followed by manual correction for final optimization. Other acquisition parameters were: TR=3000 ms, TE=42.26 ms, sweep width=4960 Hz, number of points=256, and 4 repetitions for signal averaging. Respiratory and cardiac gating were employed to improve signal stability[26]. Total acquisition time was approximately 3 minutes, varying slightly by respiratory rate. Additional FP-DDE acquisitions were acquired in 35 rats at 2 vertebral levels above and below the lesion epicenter using these same parameters to determine the ability of this technique for collecting data remote from the injury site.

In a subset of the injured animals, application of the filter-probe contrast mechanism was combined with an imaging readout along with a reduced view (rFOV) excitation scheme[29] implemented as an echo planar gradient trajectory with 16 excitation Gaussian sub-pulses, each with 0.2 ms duration. This acquisition had TE=35 ms, field of view of 13.5×9.6 mm^2 (90×64 matrix: 150 μm^2 in-plane resolution) and 2 mm slice thickness and did not include additional outer volume suppression or fat suppression. The diffusion scheme was identical to the DDE except only five probe b-values were used ranging from 0–1000 s/mm^2. Acquisition time was approximately 5:30 minutes, varying slightly by respiratory rate. A comparison of DTI and filter-probe images is shown in Figure 1.

MRI Analysis

An overview of the DTI and FP-DDE analysis is given in Figure 2. DW-EPI data were motion and eddy current corrected using the Spinal Cord Toolbox[30]. DTI parameter maps[10, 11] were calculated using weighted linear least squares implemented in FSL[31], generating maps of DTI parameters of mean diffusivity (MD), axial diffusivity (AD), radial

diffusivity (RD), and fractional anisotropy (FA). Whole cord regions of interest (ROI) were manually traced using parameter maps and the non-diffusion weighted (b=0 s/mm^2) images. To avoid inclusion of voxels with CSF, the manual ROIs were masked by diffusion weighted images perpendicular to the spinal cord (b=250 s/mm^2). The reported mean DTI parameter values consist of the average of the 4 slices centered at the lesion site and spanning the same extent of spinal cord as the FP-DDE voxel.

These diffusion data were also processed using the White Matter Tract integrity (WMTI) model[21, 32, 33], which utilizes the multiple b-value shells and directions in order to model the fraction of axonal water (AWF)based on the following equation:

$$AWF = \frac{K_{max}}{K_{max} + 3} \quad [1]$$

where K_{max} is the maximum kurtosis[34, 35] over all possible directions, given as

$$S_b = S_0 \cdot \exp\left(-bD + \frac{1}{6}b^2D^2K\right) \quad [2]$$

The diffusion tensors for each compartment were derived, with the diffusion of the intra-axonal space (D_a) given by

$$D_{a,n} = D_n\left[1 - \sqrt{\frac{K_n(1 - AWF)}{3 \cdot f_{intra}}}\right] \quad [3]$$

where D_n and K_n are the diffusion and kurtosis in a given direction n, and the diffusion of the extra-axonal space given by

$$D_{e,n} = D_n\left[1 + \sqrt{\frac{K_n \cdot AWF}{3(1 - AWF)}}\right] \quad [4]$$

Analysis of FP-DDE data used custom Matlab scripts for automated derivation of diffusion parameters from the magnitude of the filtered diffusion signal as previously reported[26]. For similarity to DTI, the FP-DDE signals were fit to a standard monoexponential diffusion equation:

$$S_i = S_0 \cdot \exp\left(-b \cdot ADC_{\parallel}\right) \quad [5]$$

where S_i is the diffusion-weighted signal, S_0 is the non-diffusion weighted signal, b is the diffusion weighting b-value, and $ADC_{\parallel}$ is the parallel diffusivity. Only the "probe" diffusion weighting values were considered, so S_0 reflects the signal from the first filtered point (filter b=2000 s/mm^2 and probe b=0 s/mm^2). Since restricted diffusion also exhibited high sensitivity to injury, a bi-exponential equation was used to model two non-exchanging compartments:

$$S_i = S_0 \cdot f_R \cdot \exp(-b \cdot D_R) + S_0(1 - f_R) \exp\left(-b \cdot D_{fast}\right) \quad [6]$$

where D_R and D_{fast} represent the restricted and non-restricted diffusivities, respectively, and f_R is the fraction of signal (0–1) with restricted diffusion. All fitting used a constrained maximum diffusivity of 3.0 μm^2/ms.

For rFOV filter-probe images, maps of parallel diffusivity ($ADC_{\parallel}$) along the spinal cord were calculated with Eq. 5 using only the filtered images. Parameter maps were derived from a single slice at the T10 injury epicenter. Color-coded composite images were generated to simultaneously visualize acute axonal injury and axonal loss based on $ADC_{\parallel}$ (red; 0–2 μm^2/ms) and SNR-normalized $DWI_{\perp}$ image (green; 0–30 units of signal to noise ratio), respectively.

Functional Scoring

The Basso, Beattie, and Breshnahan locomotor scale[36, 37], which scores hind limb locomotor function in an open field testing procedure, was used to evaluate functional status of rats at 1 and 30 days post injury (dpi). Video recordings of each session were scored by two trained individuals blinded to injury severity and dpi, with the mean score used for subsequent analysis.

Histological Quantification

Histological sectioning and staining was performed in 37 rats (MCW:18, NU: 19). Immediately following 30-day imaging and functional scoring, rats were euthanized with phenobarbital euthanasia followed by transcardial perfusion with phosphate buffered saline (PBS) and fixation with 4% paraformaldehyde in PBS. The spinal column was maintained in fixative for 48 hours and the spinal cord was subsequently removed from the column and processed for histology by embedding in paraffin. From the injury site, transverse 5 μm thick sections were cut and stained for primary antibodies to: phosphorylated anti-neurofilament H (SMI31; BioLegend, San Diego, CA) indicative of healthy axons, non-phosphorylated neurofilament H (SMI-32; BioLegend, San Diego, CA) indicative of injured axons, anti-CD68 (ED1; Abcam, Cambridge, MA) for activated microglia, anti-glial fibrillary acidic protein (GFAP; EMD Millipore, Darmstadt, Germany) for astrocytes, and DAPI DNA staining (Vector Laboratories, Burlingame, CA) for cell nuclei as a measure of overall cellularity.

Fluorescent images of each section were acquired using a 20× objective with a resolution of 0.32 μm/pixel. Images were analyzed with ImageJ[38] using the Analyze Particles plugin

along with custom macros for cell counting. For each stain, a region of interest was manually placed around the entire spinal cord section. Background signal was removed using an intensity-based percentile cutoff (ranging from 95–98%) and positively-stained cells were identified with a minimum size threshold (ranging from 155 μm for SMI31 to 1100 μm for SMI32) and circularity constraints (ranging from 0.1–1.0 for ED1 to 0.0–0.6 for GFAP) to remove spurious pixels. Total counts of positively-stained cells for all antibodies were normalized by the total cord area and log-transformed for subsequent analysis.

Statistical Analysis

All statistical analysis was performed using Stata 12 (StataCorp. 2011. Stata Statistical Software: Release 12. College Station, TX: StataCorp LP). The relationship between imaging metrics and BBB scores were analyzed using a linear regression model to determine the predictive ability of early imaging for long-term functional outcome. Regression analysis was repeated by omitting the sham group to further evaluate separation of injury severities. Site was included as a covariate and reported for those metrics where it had a significant effect ($p < 0.01$). The best-performing diffusion metrics from the FP-DDE and DTI schemes were further compared for strength of correlation with BBB scores using Steiger's test[39], which involves a Fisher r-to-z transformation to provide a z-score with which to test correlation equality. Prediction models for chronic BBB scores were also compared using a likelihood ratio test to evaluate the relative strengths of models using acute BBB alone, acute diffusion measurements alone, or a combination of acute BBB and diffusion measures. Histological outcomes were related to acute and chronic diffusion metrics and BBB scores using multiple linear regression of stained cell counts as independent variables. Experimental site (MCW, NU) was also included as a covariate and reported for those metrics where it had a significant contribution ($p < 0.01$).

In the reported data, two animals were excluded due to failed drop procedures, three rats died after data collection at the acute time point and were not included in chronic analysis, and three rats had scans excluded due to poor data quality.

Results

Relationship with Functional Outcomes

Results of all regression analyses for functional scores with diffusion metrics are presented in Table 1. The acute diffusion metrics of $ADC_\parallel$, f_R, FA, AD, D_a, and D_{Epar} showed significant relationships with acute BBB scores, although significance was not maintained with the sham group omitted. Similarly, all chronic diffusion metrics showed significant relationships with chronic BBB scores except for MD, although again significance was not maintained with the sham group omitted. Finally, all acute diffusion metrics demonstrated significant relationships with chronic BBB scores except for RD, AWF, and D_{Eperp} (Fig. 3, Table 1). All chronic diffusion parameters showed the same correlation directionality as the acute diffusion metrics, with the exception of chronic RD, MD, and D_{Eperp}, which were negatively correlated with chronic BBB scores. The DTI metric from the acute time point that best predicted chronic BBB scores (AD: $R^2 = 0.52$) was compared with FP-DDE metrics

(ADC$_{||}$: R^2=0.63) and using the Steiger's z test, showing no significant difference in predictive power compared to acute ADC$_{||}$ (Z=1.07, two-tailed p=0.28). Similar results were seen with no difference between ADC$_{||}$ and D$_a$ from WMTI (Z=0.74, 2-tailed p=0.46).

Likelihood ratio tests were used to compare goodness-of-fit of predictive models of chronic BBB scores, including acute BBB score alone (R^2=0.71, p<0.0001), acute ADC$_{||}$ alone (R^2=0.63, p<0.0001), and a combination of acute ADC$_{||}$ and acute BBB (R^2=0.77, p<0.0001). It was found that the combined acute ADC$_{||}$ and BBB model outperformed acute BBB alone (χ^2=11.61, p=0.0007) and acute ADC$_{||}$ alone (χ^2=25.28, p<0.0001) for predicting chronic BBB scores. Similarly, models testing acute BBB alone, acute f_R alone (R^2=0.55, p<0.0001), and a combination of acute f_R and acute BBB scores (R^2=0.77, p<0.0001) found that the model combining acute f_R and BBB predicted chronic BBB scores better than acute BBB alone (χ^2=10.30, p=0.001) or acute f_R alone (χ^2=32.93, p<0.0001). For the combined acute BBB and diffusion prediction model both acute ADC$_{||}$ (β=0.36) and acute f_R (β=−0.31) substantially contributed to the prediction. Similarly, the model combining acute AD and acute BBB scores (R^2=0.78, p<0.0001) was a better predictor of chronic BBB score than acute BBB alone (χ^2=14.17, p=0.0002), as was a combination of Da and acute BBB (Regression: R^2=0.75, p<0.0001; Likelihood Ratio Test: (χ^2=7.82, p=0.005).

For assessments remote from the lesion, 29 animals had scans two vertebral levels rostral to the injury epicenter, which showed a non-significant association of acute ADC$_{||}$ with acute BBB scores (R^2=0.19, p=0.02) and with chronic BBB score (R^2=0.21, p=0.02), noting that the strength of the relationship was much lower than at the lesion epicenter. The correlation coefficient between the rostral diffusion data and that from the epicenter was 0.66 for the acute data (R^2=0.29, p=0.002) and 0.42 for the chronic data (R^2=0.08, p=0.16). Acute ADC$_{||}$ data collected two vertebral segments caudal to the injury site (n=35) did not show a significant relationship to acute BBB score (R^2=0.12, p=0.04) or chronic BBB score (R^2=0.07, p=0.13). The correlation coefficient between the caudal diffusion data and that from the epicenter was 0.33 for the acute data (R^2=0.20, p=0.006) and 0.34 for the chronic data (R^2=0.06, p=0.29). Distance from the lesion site included as a variable in these analyses showed no significance in relating to BBB scores in the acute or chronic period.

Relationship with Histological Outcomes

Examples of histological stains in sham and severely injured rats are given in Figure 4a. Overall, the SCI lesion site was associated with fewer healthy axons (SMI31), but increased injured axons (SMI32), activated macrophages (ED1), cellularity (DAPI), and astrocyte reactivity (GFAP). Multiple linear regression results are presented in Table 2.

For prediction of histological outcomes from acute diffusion metrics, ADC$_{||}$ showed a strong relationship to histology overall (R^2=0.68, p<0.0001) and was significantly related to SMI32 staining for injured axons (p=0.001, β=−0.64). Similarly, acute f_R (R^2=0.55, p=0.0001) also showed a significant relationship SMI31 cell counts (p=0.01, β=0.57). While acute FA (R^2=0.71, p<0.0001) and AD (R^2=0.59, p<0.0001) showed strong overall relationships with histology, neither showed significance with specific cellular markers. From the WMTI model, D$_a$ (R^2=0.71, p<0.0001) and D$_{Epar}$ (R^2=0.71, p<0.0001) were significantly related to

histology overall, with significant associations between D_a and DAPI staining (p=0.004, β= −0.42) and between D_{Epar} and ED1 staining (p=0.007, β=−0.45). While the multiple regression analysis of chronic diffusion metrics identified significance in chronic $ADC_∥$, FA, AD, RD, AWF, D_a, D_{Epar}, and D_{Eperp} (Table 2), significance with specific cellular markers was only observed between FA and SMI32 (p<0.001, β=−0.70) and between D_a and SMI32 (p=0.001, β=−0.70).

As a related test of the relationship between histological markers and functional outcome, multiple linear regression was performed with these same markers and BBB scores. Both acute BBB scores (R^2=0.72, p<0.0001) and chronic BBB scores (R^2=0.63, p<0.0001) had a significant relationship with SMI32 cell counts (Acute: p<0.001, β=−0.69; Chronic: p=0.004, β=−0.67) while no other cellular markers had a significant independent relationship to BBB scores. A graphical representation comparing these relationships with those from diffusion metrics is given in Figure 4b.

Filter-Probe Imaging

Example rFOV filter-probe images are shown in Figure 5. Combination of the perpendicular filtered diffusion image ($DWI_⊥$) and parallel diffusivity ($ADC_∥$) as a composite color map enabled simultaneous visualization of axonal injury and loss. Acutely at the lesion site, axonal injury without loss was evident (high $DWI_⊥$ signal and low $ADC_∥$) as an increased red area which scales with the degree of injury. At 30 days post-injury, these acute injured regions formed a central cystic cavity visible as a bright CSF on T_2-weighted images and a void on composite images. No axonal injury was evident at 30 days post-injury, but the residual tissue in the severe injury demonstrated a decrease in axonal density (low $DWI_⊥$ signal). Subsequent histological staining for SMI31 and SMI32 axons confirmed cavitation with increased axonal injury (SMI32) and decreased healthy axonal density (SMI31) in the severe injury. Comparison over time showed strong agreement between localized areas of damage measured acutely with the FP-DDE and chronic loss of axons related to the severity of the induced injury.

Comparison of Experimental Sites

To examine potential effects of MRI system differences between experimental locations, noting that the systems were the same field strength and vendor but different software version and all other experimental procedures were performed by the same personnel, all statistical tests included experimental site as an independent variable. In the ANOVA for categorical effects of injury severity, the DTI metric of acute FA showed a significant interaction between site and severity (p=0.004) as well as the WMTI metrics of acute D_a (p=0.001) and acute D_{Epar} (p=0.001). For regression analyses of acute diffusion metrics with acute BBB score, a significant effect of site was seen with AD (p=0.009) and $ADC_∥$ (p=0.003). For regression of chronic diffusion metrics and chronic BBB score, AWF showed a significant site effect (p=0.01). No significant site effect was seen for regression of acute diffusion metrics with chronic BBB scores. For the histological regression analyses, significant site effect was seen for the acute metrics of ADC∥ (p<0.001), AD (p<0.001), RD (p<0.001), MD (p<0.001), AWF (p<0.001), and D_{Eperp} (p<0.001). For chronic diffusion

metrics with chronic histology, a significant site effect was seen with ADC∥ (p=0.01). No site effect was seen for BBB scores in the histology analysis.

Discussion

Overall, these results demonstrate that the acute filter-probe diffusion MRI technique shows a strong association with functional and histological domains that predict outcome in a rat model of SCI. Moreover, it shows a distinct benefit over DTI with faster acquisition (<4 mins) and a fully automated analysis of the spectroscopic data that is objective and easily interpretable. Benefits were also seen in the filter-probe imaging at the lesion site, which provided high contrast maps to distinguish axonal injury and loss from healthy spinal cord white matter tissue, which was further enhanced by the removal of contaminating signals from CSF and cystic formations that obscure DTI maps. Thus, this study demonstrated multiple strengths of the filter-probe technique, demonstrating promise as a biomarker of spinal cord injury severity with potential for use in acute clinical evaluation.

As demonstrated previously[26], the filter-probe technique demonstrated its ability to predict functional outcome with high accuracy. Metrics from FP-DDE, DTI, and WMTI were significantly related to BBB scores at both acute and chronic time points, indicating the ability of each technique to detect the presence of acute and chronic injuries. The omission of the sham groups demonstrated that acute diffusion metrics were not reliable marker of functional impairment in the acute period, but they were strong predictive markers of later functional outcomes and may provide use in clinical prognostication of SCI outcome. While FP-DDE was similarly predictive to DTI and WMTI, its analysis required much less manual involvement in post-processing and analysis. Lastly, combining acute FP-DDE metrics and acute BBB scores improved the predictive ability for chronic BBB scores, indicating potential usefulness when added to clinical functional testing. Thus, acute FP-DDE metrics provide a useful metric with a distinct advantage over DTI and WMTI for predicting chronic functional outcomes while retaining a significant relationship to axonal damage.

To explore the cellular basis of the delay between diffusion metrics and functional scoring, quantitative histology was related to the diffusion metrics. As expected, BBB scores were significantly related to the extent of axonal injury (SMI32 staining), as axonal injury and sparing are consistently shown to correlate with function in experimental SCI models[8, 9, 37, 40–42]. Acute ADC∥ from FP-DDE was also significantly correlated with chronic SMI32 positive cell counts indicative of axonal damage, highlighting its prognostic accuracy for pathological features. This agrees with previous work showing relationships between longitudinal ADC and degree of axonal loss[16, 43]. In this study, no acute DTI metrics showed a significant and independent relationship with chronic histological markers of axonal injury or other cellular markers of damage. Acute WMTI metrics were significant predictors for cellularity (D_a and DAPI) and with activated microglia (D_{Epar} and ED1). However, in the chronic setting, both DTI and WMTI were associated with distinct pathological features in which FA and D_a were closely related to axonal damage while FP-DDE metrics were not. These features highlight the specificity of FP-DDE for acute axonal injury, for which it was designed, by capturing early axon morphological changes without complications from edema[19].

This technique was designed to relate more specifically to axonal injury as it is the pathological feature most indicative of long-term outcome[8, 9, 37, 40–42]. Previous studies demonstrated the utility of DTI in the hyperacute period following injury[17, 44], although these studies highlighted a murine model at a period prior to the onset of edema. Edema is a characteristic feature of clinical SCI, and is a dynamic and evolving process[45] that can have a confounding influence on the specificity to axonal injury in DTI[19]. By suppressing the signals associated with extracellular fluid, FP-DDE is more robust against the effects of edema. Early measures of $ADC_{\parallel}$ are likely capturing the extent of axonal beading previously hypothesized to occur in acute trauma[12] and directly observed in the *in vivo* SCI cord[46]. Thus, prognostication in the acute setting was the major impetus for these studies and fulfills a precise clinical need.

On the other hand, the complex and evolving cellular landscape of axon degeneration and other inflammatory processes in SCI demonstrate significant change over the 30 days examined with this study[47, 48]. As the current results demonstrate, the utility of FP-DDE to monitor axonal injury decreases over time. For instance, FP-DDE in the chronic setting did not correlate with histological markers and the filter-probe images at 30 days post-injury (Fig. 5) did not suggest detection of acute injury (red color on DW-combined image). On the other hand, both the loss of spinal cord tissue and decreased axonal density in the spared tissue was evident in both histological sections. The degeneration of axons and increased vacuolization at the injury site render the technique less effective at the chronic time point[49, 50] These results are consistent with other acute neurological injuries, most notably in cerebral ischemia. DWI is a highly sensitive marker of an acute infarct, but its sensitivity diminishes up to the first week post-injury as diffusion pseudo-normalizes. These imaging signatures are paralleled by degeneration, inflammatory cell infiltration, and tissue loss, which follows a similar cascade in SCI. At the chronic stage, the number of residual axons through the lesion is closely associated with functional status[8, 9]. While FP-DDE is indicative of axonal injury, beyond this acute window its sensitivity to injury diminishes. Additional follow-up is warranted to identify this window with higher frequency serial studies[51]. On the other hand, DTI measures such as FA and WMTI measures such as D_a have stronger relationships with axonal loss (Fig. 4) and are likely to perform better as markers of chronic SCI indicative of axonal sparing. Ongoing monitoring of SCI or evaluation of therapeutics may therefore require a combination of techniques, including DTI, noting that these relationships change over time and, as such, must be carefully studied within this context.

One important barrier for clinical adoption of MRI techniques including diffusion is their ability monitor the injury after surgical implantation of spinal hardware. At the lesion site, metal hardware causes artifacts that preclude their use. One approach to overcome this complication is to image remote from the site of injury, including adjacent to the hardware several vertebral segments above the lesion in the spinal cord[52–54] and even using brain changes as a surrogate for those in the lesion site[55, 56]. We evaluated FP-DDE two vertebral segments rostral or caudal to the injury epicenter in subset of animals. The results demonstrate that measurements rostral to the injury were modestly correlated with those taken at the injury site. Consequently, these remote measurements were significantly predictive of functional outcomes, but with markedly less accuracy then at the lesion site.

These results have implications for long-term follow up in SCI. First, imaging remote from the lesion site is an alternative in the case of surgical hardware that relates to injury. However, monitoring the lesion site provides the strongest relationships to subsequent neurological outcomes, as might be expected. The capability to image near metal hardware has advanced in recent years[57], and diffusion MRI contrast is also emerging but still in early stages[58]. Further advances and solutions for SCI are needed to overcome these significant challenges.

FP-DDE has theoretical and practical advantages over existing MRI measures, including DTI. However, its primary limitation is that it requires alignment of the imaging plane or spectroscopy voxel with the spinal cord axis, and while this does not pose a substantial burden for the spinal cord, it must be considered. Even so, the estimates of $ADC_{\parallel}$ are within 10% of their true values with misalignment of up to 18° from the long axis of the spinal cord[59]. Moreover, the single voxel spectroscopic measure is targeted to be a whole-cord estimate of injury. The advantage is a fully automated and quantitative analysis. In traumatic injury, the deformation of the cord at the site of injury is often severe and identification of individual tracts is problematic. However, in focal injuries or other disease of the spinal cord, the spatial pattern of injury or tract-specific damage has important consequences for domain-specific impairments. As shown (Fig. 4), filter-probe contrast coupled with an imaging readout reveals the spatial pattern of injury without contamination by edema. Although the signal to noise is lower than with DTI, the contrast and specificity it provides is more critical to assessing axonal injury, which may provide clinical usefulness in radiologic planning for surgical intervention of the injury. Further in-depth investigations into the differences and applications in other spinal cord pathologies are needed to address its clinical potential.

In summary, early FP-DDE measurements show a significant advantage over DTI in predicting long-term outcome in a preclinical model of SCI, likely due to its close association with axonal injury and decreased contamination by edema. Furthermore, its use with acute functional scoring significantly improves prognostic power for long-term functional outcome in the rat. Use of this technique as an imaging or spectroscopic technique provides improved prediction of outcomes that shows potential use in both research and clinical applications of SCI.

Acknowledgments

Abbreviations

SCI   Spinal Cord Injury

DTI   Diffusion Tensor Imaging

FP-DDE   Filter-Probe Double Diffusion Encoding

WM   White Matter

CSF   Cerebrospinal Fluid

Bibliography

1. Piazza M, Schuster J. Timing of Surgery After Spinal Cord Injury. Neurosurg Clin N Am. 2017; 28(1):31–9. [PubMed: 27886880]

2. Kirshblum SC, Botticello AL, Benaquista DeSipio G, Fichtenbaum J, Shah A, Scelza W. Breaking the news: A pilot study on patient perspectives of discussing prognosis after traumatic spinal cord injury. J Spinal Cord Med. 2016; 39(2):155–61. [PubMed: 25897890]

3. Kirshblum SC, Burns SP, Biering-Sorensen F, et al. International standards for neurological classification of spinal cord injury (revised 2011). J Spinal Cord Med. 2011 Nov; 34(6):535–46. [PubMed: 22330108]

4. Fawcett JW, Curt A, Steeves JD, et al. Guidelines for the conduct of clinical trials for spinal cord injury as developed by the ICCP panel: spontaneous recovery after spinal cord injury and statistical power needed for therapeutic clinical trials. Spinal Cord. 2007 Mar; 45(3):190–205. [PubMed: 17179973]

5. Bozzo A, Marcoux J, Radhakrishna M, Pelletier J, Goulet B. The role of magnetic resonance imaging in the management of acute spinal cord injury. Journal of neurotrauma. 2011 Aug; 28(8): 1401–11. [PubMed: 20388006]

6. Kim SY, Shin MJ, Chang JH, et al. Correlation of diffusion tensor imaging and phase-contrast MR with clinical parameters of cervical spinal cord injuries. Spinal Cord. 2015 Aug; 53(8):608–14. [PubMed: 25868880]

7. Wilson JR, Grossman RG, Frankowski RF, et al. A clinical prediction model for long-term functional outcome after traumatic spinal cord injury based on acute clinical and imaging factors. Journal of neurotrauma. 2012 Sep; 29(13):2263–71. [PubMed: 22709268]

8. Ferguson AR, Irvine KA, Gensel JC, et al. Derivation of multivariate syndromic outcome metrics for consistent testing across multiple models of cervical spinal cord injury in rats. PloS One. 2013; 8(3):e59712. [PubMed: 23544088]

9. Medana IM, Esiri MM. Axonal damage: a key predictor of outcome in human CNS diseases. Brain. 2003 Mar; 126(Pt 3):515–30. [PubMed: 12566274]

10. Basser PJ, Mattiello J, LeBihan D. Estimation of the effective self-diffusion tensor from the NMR spin echo. J Magn Reson B. 1994 Mar; 103(3):247–54. [PubMed: 8019776]

11. Basser PJ, Pierpaoli C. A simplified method to measure the diffusion tensor from seven MR images. Magn Reson Med. 1998 Jun; 39(6):928–34. [PubMed: 9621916]

12. Budde MD, Frank JA. Neurite beading is sufficient to decrease the apparent diffusion coefficient after ischemic stroke. Proc Natl Acad Sci U S A. 2010 Aug 10; 107(32):14472–7. [PubMed: 20660718]

13. Coleman M. Axon degeneration mechanisms: commonality amid diversity. Nat Rev Neurosci. 2005 Nov; 6(11):889–98. [PubMed: 16224497]

14. Tu TW, Frank JA. Assessing White Matter Integrity in Experimental Spinal Cord Injury Using Diffusion Tensor Imaging. J Neurosci Neuroeng. 2013; 2(5):415–30.

15. Budde MD, Kim JH, Liang HF, et al. Toward accurate diagnosis of white matter pathology using diffusion tensor imaging. Magn Reson Med. 2007; 57(4):688–95. [PubMed: 17390365]

16. Kim JH, Loy DN, Liang HF, Trinkaus K, Schmidt RE, Song SK. Noninvasive diffusion tensor imaging of evolving white matter pathology in a mouse model of acute spinal cord injury. Magn Reson Med. 2007 Aug; 58(2):253–60. [PubMed: 17654597]

17. Kim JH, Loy DN, Wang Q, et al. Diffusion Tensor Imaging at 3 Hours after Traumatic Spinal Cord Injury Predicts Long-Term Locomotor Recovery. Journal of neurotrauma. 2010; 27:587–98. [PubMed: 20001686]

18. Loy DN, Kim HA, Xie M, Schmidt RE, Trinkaus K, Song SK. Diffusion tensor imaging predicts hyperacute spinal cord injury severity. Journal of neurotrauma. 2007; 24(6):979–90. [PubMed: 17600514]

19. Skinner NP, Kurpad SN, Schmit BD, Budde MD. Detecting Acute Nervous System Injury with Advanced Diffusion Weighted MRI: A Simulation and Sensitivity Analysis. NMR Biomed. 2015; 28(11):1489–506. [PubMed: 26411743]

20. Alexander DC, Hubbard PL, Hall MG, et al. Orientationally invariant indices of axon diameter and density from diffusion MRI. NeuroImage. 2010 Oct 1; 52(4):1374–89. [PubMed: 20580932]

21. Fieremans E, Benitez A, Jensen JH, et al. Novel white matter tract integrity metrics sensitive to Alzheimer disease progression. AJNR American journal of neuroradiology. 2013 Nov; 34(11): 2105–12. [PubMed: 23764722]

22. Grussu F, Schneider T, Zhang H, Alexander DC, Wheeler-Kingshott CA. Neurite orientation dispersion and density imaging of the healthy cervical spinal cord in vivo. NeuroImage. 2015 May 1.111:590–601. [PubMed: 25652391]

23. Pasternak O, Sochen N, Gur Y, Intrator N, Assaf Y. Free water elimination and mapping from diffusion MRI. Magn Reson Med. 2009 Sep; 62(3):717–30. [PubMed: 19623619]

24. Wang Y, Wang Q, Haldar JP, et al. Quantification of increased cellularity during inflammatory demyelination. Brain. 2011 Dec; 134(Pt 12):3590–601. [PubMed: 22171354]

25. Zhang H, Schneider T, Wheeler-Kingshott CA, Alexander DC. NODDI: practical in vivo neurite orientation dispersion and density imaging of the human brain. NeuroImage. 2012 Jul 16; 61(4): 1000–16. [PubMed: 22484410]

26. Skinner NP, Kurpad SN, Schmit BD, Muftuler TL, Budde MD. Rapid In Vivo Detection of Rat Spinal Cord Injury with Double-Diffusion-Encoded Magnetic Resonance Spectroscopy. Magn Reson Med. 2016; 77(4):1639–49. [PubMed: 27080726]

27. Yang G, Tian Q, Leuze C, Wintermark M, McNab JA. Double diffusion encoding MRI for the clinic. Magn Reson Med. 2017 Dec 19.

28. Hasan KM, Parker DL, Alexander AL. Comparison of Gradient Encoding Schemes for Diffusion Tensor MRI. J MRI. 2011; 13:769–80.

29. Saritas EU, Cunningham CH, Lee JH, Han ET, Nishimura DG. DWI of the spinal cord with reduced FOV single-shot EPI. Magn Reson Med. 2008; 60(2):468–73. [PubMed: 18666126]

30. De Leener B, Lévy S, Dupont SM, et al. SCT: Spinal Cord Toolbox, an open-source software for processing spinalcord MRI data. NeuroImage. 2017; 145A:24–43.

31. Jenkinson M, Beckmann CF, Behrens TE, Woolrich MW, Smith SM. FSL. NeuroImage. 2012; 62:782–90. [PubMed: 21979382]

32. Fieremans E, Jensen JH, Helpern JA. White matter characterization with diffusional kurtosis imaging. NeuroImage. 2011 Sep 1; 58(1):177–88. [PubMed: 21699989]

33. Jelescu IO, Veraart J, Adisetiyo V, Milla SS, Novikov DS, Fieremans E. One diffusion acquisition and different white matter models: How does microstructure change in human early development based on WMTI and NODDI? NeuroImage. 2015 Feb 15.107:242–56. [PubMed: 25498427]

34. Hui ES, Cheung MM, Qi L, Wu EX. Towards better MR characterization of neural tissues using directional diffusion kurtosis analysis. NeuroImage. 2008 Aug 1; 42(1):122–34. [PubMed: 18524628]

35. Jensen JH, Helpern JA. MRI quantification of non-Gaussian water diffusion by kurtosis analysis. NMR Biomed. 2010 Aug; 23(7):698–710. [PubMed: 20632416]

36. Basso DM, Beattie MS, Bresnahan JC. A Sensitive and Reliable Locomotor Rating Scale for Open Field Testing in Rats. J Neurotrauma. 1995; 12(1):1–21. [PubMed: 7783230]

37. Basso DM, Beattie MS, Bresnahan JC. Graded Histological and Locomotor Outcomes after Spinal Cord Contusion Using the NYU Weight-Drop Device versus Transection. Experimental Neurology. 1996; 139:244–56. [PubMed: 8654527]

38. Rasband WS. Image Processing and Analysis in Java (ImageJ). Bethesda, Maryland, USA: U. S. National Institutes of Health; 1997–2014. http://imagejnihgov/ij/

39. Steiger J. Tests for comparing elements of a correlation matrix. Psychological Bulletin. 1980; 87:245–51.

40. Chen K, Liu J, Assinck P, et al. Differential Histopathological and Behavioral Outcomes Eight Weeks after Rat Spinal Cord Injury by Contusion, Dislocation, and Distraction Mechanisms. Journal of neurotrauma. 2016; 33(18):1667–84. [PubMed: 26671448]

41. Hase T, Kawaguchi S, Hayashi H, Nishio T, Mizoguchi A, Nakamura T. Spinal cord repair in neonatal rats: a correlation between axonal regeneration and functional recovery. Eur J Neurosci. 2002; 15(6):969–74. [PubMed: 11918656]

42. Navarro R, Juhas S, Keshavarzi S, et al. Chronic spinal compression model in minipigs: a systematic behavioral, qualitative, and quantitative neuropathological study. Journal of neurotrauma. 2012; 29(3):499–513. [PubMed: 22029501]

43. Schwartz ED, Chin C, Shumsky JD, et al. Apparent Diffusion Coefficients in Spinal Cord Transplants and Surrounding White Matter Correlate with Degree of Axonal Dieback After Injury in Rats. AJNR Am J Neuroradiol. 2005; 26:7–18. [PubMed: 15661691]

44. Kim HA, Song SK, Magnuson DS. Comprehensive Locomotor Outcomes Correlate to Hyperacute Diffusion Tensor Measures After Spinal Cord Injury in the Adult Rat. Experimental Neurology. 2012; 235(1):188–96. [PubMed: 22119625]

45. Leypold BG, Flanders AE, Burns AS. The early evolution of spinal cord lesions on MR imaging following traumatic spinal cord injury. AJNR Am J Neuroradiol. 2008; 29(5):1012–6. [PubMed: 18296550]

46. Williams PR, Marincu BN, Sorbara CD, et al. A recoverable state of axon injury persists for hours after spinal cord contusion in vivo. Nat Commun. 2014 Dec 16.5:5683. [PubMed: 25511170]

47. Beck KD, Nguyen HX, Galvan MD, Salazar DL, Woodruff TM, Anderson AJ. Quantitative analysis of cellular inflammation after traumatic spinal cord injury: evidence for a multiphasic inflammatory response in the acute to chronic environment. Brain. 2010 Feb; 133(Pt 2):433–47. [PubMed: 20085927]

48. PP, PW, BS. Cellular Inflammatory Response after Spinal Cord Injury in Sprague-Dawley and Lewis Rats. J Comp Neurol. 1997; 377:443–64. [PubMed: 8989657]

49. Bramlett HM, Dietrich WD. Progressive damage after brain and spinal cord injury: pathomechanisms and treatment strategies. Neurotrauma: New Insights into Pathology and Treatment. 2007:125–41.

50. Zhang J, Jones M, DeBoy CA, et al. Diffusion tensor magnetic resonance imaging of Wallerian degeneration in rat spinal cord after dorsal root axotomy. J Neurosci. 2009 Mar 11; 29(10):3160–71. [PubMed: 19279253]

51. Buss A, Brook GA, Kakulas B, et al. Gradual loss of myelin and formation of an astrocytic scar during Wallerian degeneration in the human spinal cord. Brain. 2004 Jan; 127(Pt 1):34–44. [PubMed: 14534158]

52. Ellingson BM, Kurpad SN, Schmit BD. Ex vivo diffusion tensor imaging and quantitative tractography of the rat spinal cord during long-term recovery from moderate spinal contusion. J Magn Reson Imaging. 2008 Nov; 28(5):1068–79. [PubMed: 18972347]

53. Ellingson BM, Schmit BD, Kurpad SN. Lesion growth and degeneration patterns measured using diffusion tensor 9.4-T magnetic resonance imaging in rat spinal cord injury. J Neurosurg Spine. 2010 Aug; 13(2):181–92. [PubMed: 20672953]

54. Jirjis MB, Kurpad SN, Schmit BD. Ex vivo diffusion tensor imaging of spinal cord injury in rats of varying degrees of severity. Journal of neurotrauma. 2013 Sep 15; 30(18):1577–86. [PubMed: 23782233]

55. Freund P, Curt A, Friston K, Thompson A. Tracking changes following spinal cord injury: insights from neuroimaging. Neuroscientist. 2013 Apr; 19(2):116–28. [PubMed: 22730072]

56. Lundell H, Christensen MS, Barthelemy D, Willerslev-Olsen M, Biering-Sorensen F, Nielsen JB. Cerebral activation is correlated to regional atrophy of the spinal cord and functional motor disability in spinal cord injured individuals. NeuroImage. 2011 Jan 15; 54(2):1254–61. [PubMed: 20851198]

57. Kaushik SS, Karr R, Runquist M, et al. Quantifying metal-induced susceptibility artifacts of the instrumented spine at 1.5T using fast-spin echo and 3D-multispectral MRI. J Magn Reson Imaging. 2017 Jan; 45(1):51–8. [PubMed: 27227824]

58. Koch KM, Bhave S, Gaddipati A, et al. Multispectral diffusion-weighted imaging near metal implants. Magn Reson Med. 2018 Feb; 79(2):987–93. [PubMed: 28470795]

59. Jespersen SN, Kroenke CD, Ostergaar L, Ackerman JJH, Yablonskiy DA. Modeling dendtrite density from magnetic resonance diffusion measurements. NeuroImage. 2007; 34:1473–86. [PubMed: 17188901]
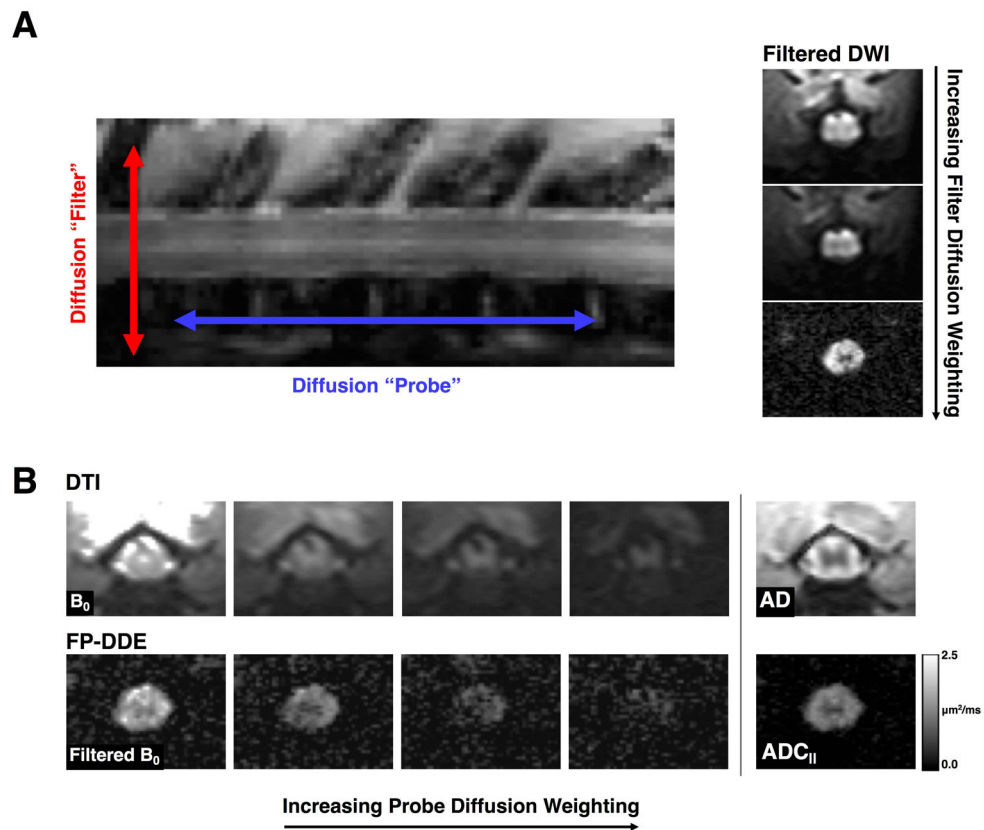
Figure 1. Filter-Probe Diffusion Weighting

(A) The "filter" and "probe" diffusion weighting directions as used in the FP-DDE collection scheme (left). By increasing the filter diffusion weighting, tissue outside of the spinal cord is attenuated prior to sampling diffusion along the spinal cord (right). (B) Conventional diffusion tensor imaging (DTI; top) employs a single diffusion direction for each measurement with maps of axial diffusivity (AD) reflecting diffusivity along the white matter fibers as well as including all tissue around the spinal cord. The filter-probe double diffusion encoding (FP-DDE; bottom) samples the same diffusion along the spinal cord, but does so after the filter pulse, resulting in a measurement of parallel diffusivity ($ADC_{\parallel}$). The measures of AD and $ADC_{\parallel}$ are analogous, but $ADC_{\parallel}$ maps have removed signals associated with CSF and edema and other tissue, which improves delineation of the spinal cord.
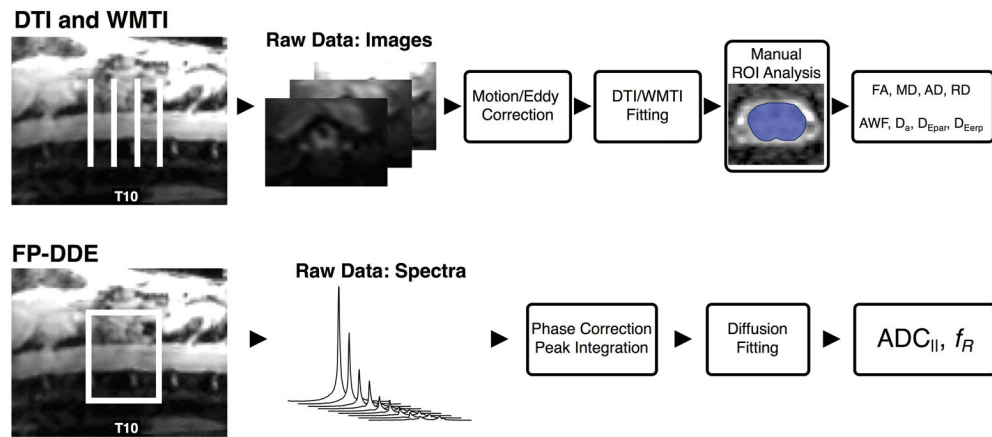
Figure 2. Diffusion Data Analysis
Acquisition and analysis scheme for diffusion tensor imaging (DTI), White Matter Tract Integrity (WMTI), and filter-probe double diffusion encoding (FP-DDE) data demonstrates slice or voxel placement over the injury epicenter. Subsequent images or spectra are then corrected and fit to a diffusion equation to produce the parameters presented in this paper. Note that while FP-DDE analysis is entirely automated as a whole-cord measure, while DTI and WMTI include a manual region of interest (ROI) drawing step to delineate the spinal cord from surrounding tissue on the parameter maps.
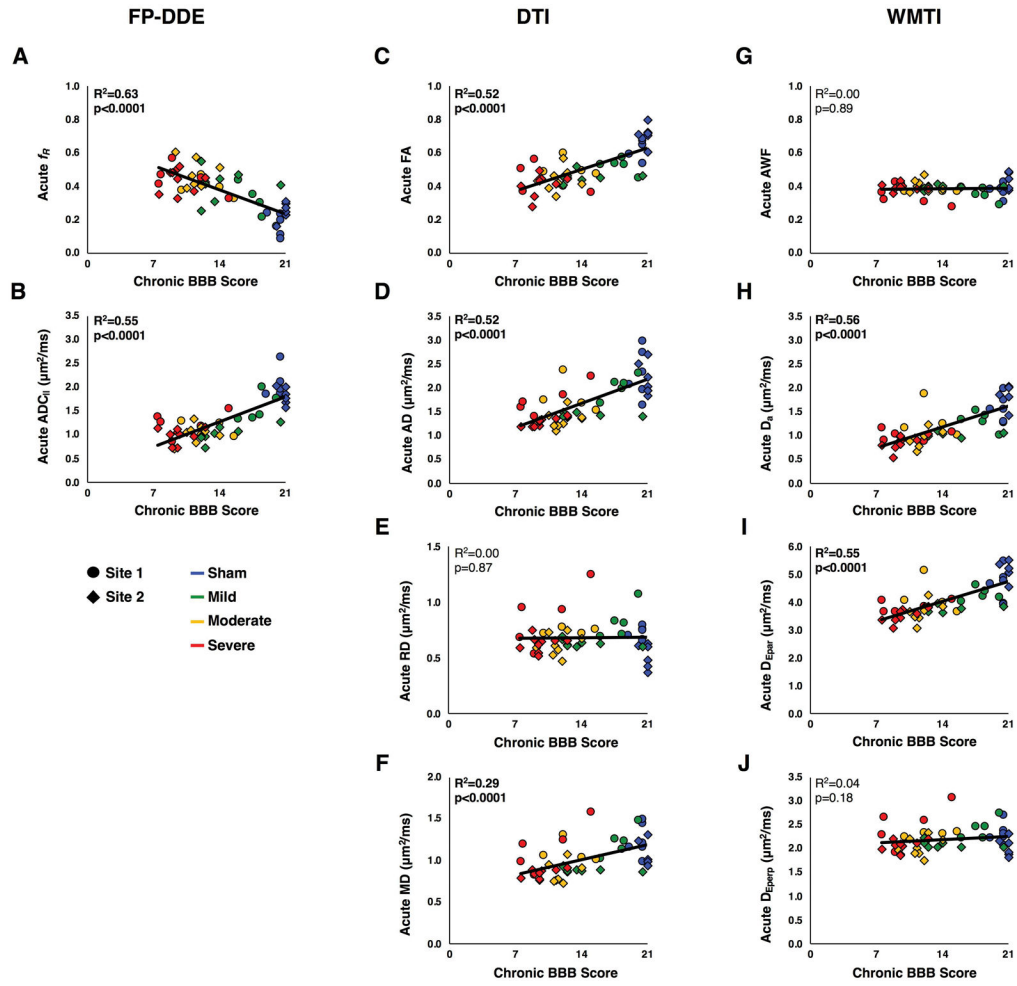
Figure 3. Chronic Outcomes Regression Analysis

Regression analyses of acute diffusion measurements with chronic BBB scores demonstrates the strong association between FP-DDE measurements and chronic functional scores. Despite the differences in amounts of data needed for fitting, FP-DDE, DTI, and WMTI all exhibit significance.
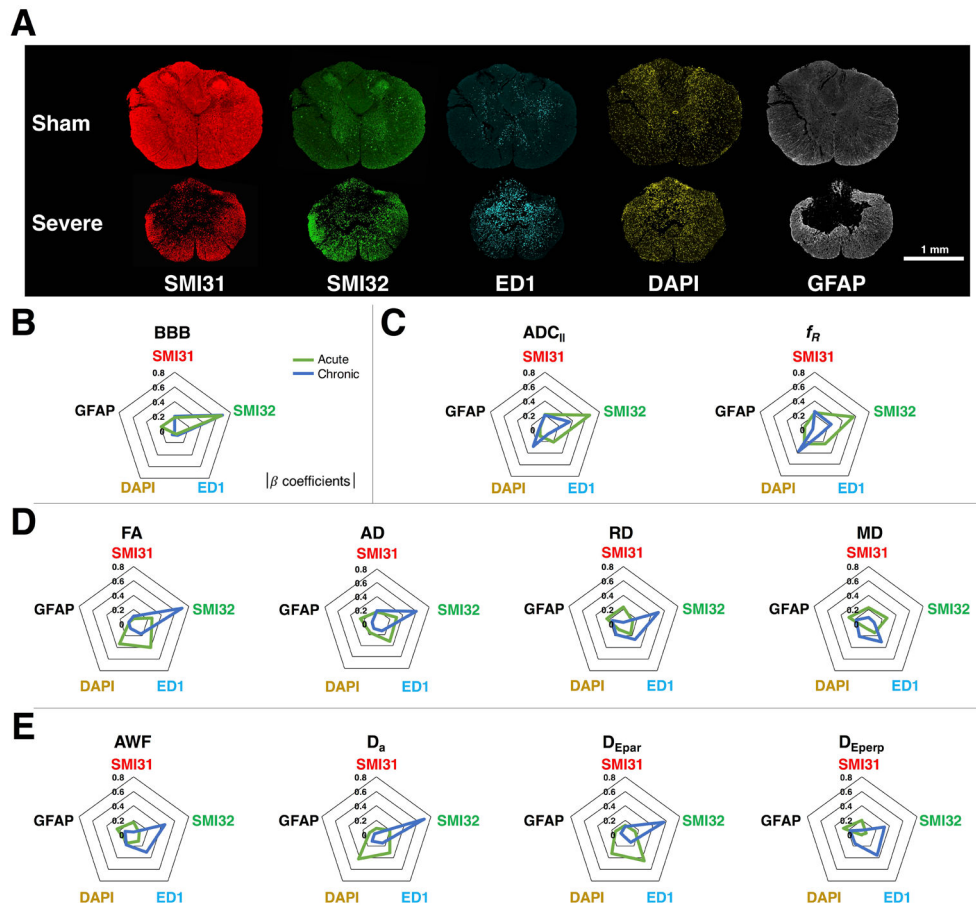
Figure 4. Histological Relationships with Diffusion Metrics

Example sham and severe histological sections obtained 30 days post-injury (A) show staining for cellular markers used in the multiple linear regression. Regression results are represented by radar plots of the absolute value of the standardized β coefficients for each histological variable. These illustrate the close relationship between axonal damage (SMI32) and BBB score (B). Acute (green) FP-DDE measures (ADC$_{\parallel}$, f_R) also predict axonal damage (SMI32) (C), whereas acute DTI metrics (FA, AD, RD, MD) and acute WMTI metrics (AWF, D$_a$, D$_{Epar}$, D$_{Eperp}$) are not strongly associated with any individual pathology (D, E). In the chronic period (blue), the findings are reversed with, where FA and Da show strong relationship to axonal damage (SMI32), but FP-DDE markers did not.
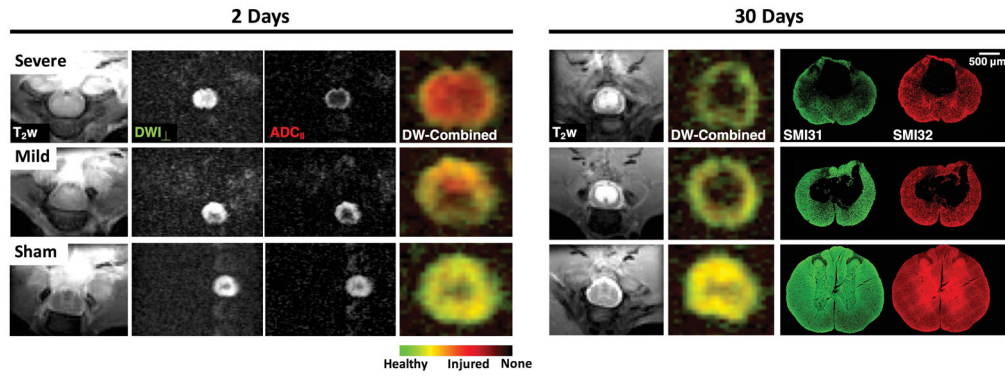
Figure 5. Filter-Probe Imaging in SCI

At 2 days post-injury, T_2-weighted hyperintensities demonstrate edema in the injured cords, but not a clear delineation of spatial extent of injury. Perpendicular weighted DW images ($DWI_\perp$) also do not readily indicate substantial changes. However, $ADC_\parallel$ maps reveal a clear injury pattern, with the severely injured rat cord having a low $ADC_\parallel$ in the center of the cord and a rim of high $ADC_\parallel$ along the periphery, and complete attenuation of non-cord signals. The mildly injured animal shows less extensive $ADC_\parallel$ changes. Composite images permit simultaneous visualization of the acute injury (red), normal axons (green/yellow), and no axons (black). In the same animals at 30 days post-injury, no acute axonal injury is evident. However, a central cystic cavity is present in both mild and severe injuries. The decreased signal within the severely-injured spared tissue (green) is suggestive of decreased axonal density and is evident in the histological stains for healthy (SMI31) and injured axons (SMI32).

Table 1

Diffusion and BBB Regression Results

Linear regression analyses for acute and chronic diffusion metrics with acute and chronic BBB scores show significance for many diffusion metrics as well as changing sensitivities over time. All data were also analyzed without sham animals to determine significance of effect within the injury groups.

Metric		Acute MRI with Acute BBB Score		Chronic MRI with Chronic BBB Score		Acute MRI with Chronic BBB Score	
		With Sham	Without Sham	With Sham	Without Sham	With Sham	Without Sham
FP-DDE	$ADC_{\parallel}$	$R^2 = 0.56$ **p < 0.0001**	$R^2 = 0.03$ p = 0.30	$R^2 = 0.29$ **p < 0.0001**	$R^2 = 0.02$ p = 0.45	$R^2 = 0.63$ **p < 0.0001**	$R^2 = 0.31$ **p = 0.0003**
	f_R	$R^2 = 0.46$ **p < 0.0001**	$R^2 = 0.05$ p = 0.17	$R^2 = 0.14$ **p = 0.008**	$R^2 = 0.00$ p = 0.71	$R^2 = 0.55$ **p < 0.0001**	$R^2 = 0.26$ **p = 0.0009**
DTI	FA	$R^2 = 0.54$ **p < 0.0001**	$R^2 = 0.03$ p = 0.33	$R^2 = 0.46$ **p < 0.0001**	$R^2 = 0.02$ p = 0.36	$R^2 = 0.52$ **p < 0.0001**	$R^2 = 0.12$ p = 0.03
	AD	$R^2 = 0.37$ **p < 0.0001**	$R^2 = 0.00$ p = 0.70	$R^2 = 0.27$ **p = 0.0001**	$R^2 = 0.10$ p = 0.06	$R^2 = 0.52$ **p < 0.0001**	$R^2 = 0.29$ **p = 0.0004**
	RD	$R^2 = 0.05$ p = 0.13	$R^2 = 0.00$ p = 0.80	$R^2 = 0.20$ **p = 0.001**	$R^2 = 0.04$ p = 0.22	$R^2 = 0.00$ p = 0.87	$R^2 = 0.11$ p = 0.04
	MD	$R^2 = 0.12$ p = 0.012	$R^2 = 0.00$ p = 0.93	$R^2 = 0.01$ p = 0.56	$R^2 = 0.08$ p = 0.09	$R^2 = 0.29$ **p < 0.0001**	$R^2 = 0.22$ **p = 0.002**
WMTI	AWF	$R^2 = 0.05$ p = 0.12	$R^2 = 0.00$ p = 0.74	$R^2 = 0.23$ **p = 0.001**	$R^2 = 0.00$ p = 0.86	$R^2 = 0.00$ p = 0.89	$R^2 = 0.08$ p = 0.09
	Da	$R^2 = 0.52$ **p < 0.0001**	$R^2 = 0.02$ p = 0.42	$R^2 = 0.35$ **p < 0.0001**	$R^2 = 0.00$ p = 0.84	$R^2 = 0.56$ **p < 0.0001**	$R^2 = 0.21$ **p = 0.003**
	De_{par}	$R^2 = 0.47$ **p < 0.0001**	$R^2 = 0.01$ p = 0.59	$R^2 = 0.33$ **p < 0.0001**	$R^2 = 0.08$ p = 0.09	$R^2 = 0.55$ **p < 0.0001**	$R^2 = 0.25$ **p = 0.001**
	De_{perp}	$R^2 = 0.00$ p = 0.86	$R^2 = 0.00$ p = 0.91	$R^2 = 0.19$ **p = 0.002**	$R^2 = 0.02$ p = 0.41	$R^2 = 0.04$ p = 0.18	$R^2 = 0.13$ p = 0.03

Table 2

Histology Multiple Linear Regression

Results of the multiple linear regression (Mult. Reg.) analysis of chronic histological staining with acute and chronic diffusion metrics and BBB scores. Standardized β coefficients are reported for each histological stain variable with significance of each indicated as *p<0.05, **p<0.01, ***p<0.005.

		Mult. Reg.	SMI31	SMI32	ED1	DAPI	GFAP
Acute Diffusion							
FP-DDE	ADC∥	R² = 0.68 **p < 0.0001**	β = 0.21	β = −0.65***	β = −0.21	β = 0.11	β = 0.07
	f_R	R² = 0.55 **p = 0.0001**	β = −0.24	β = 0.57**	β = 0.25	β = −0.25	β = −0.14
DTI	FA	R² = 0.71 **p < 0.0001**	β = −0.07	β = −0.26	β = −0.40*	β = −0.34*	β = 0.07
	AD	R² = 0.59 **p < 0.0001**	β = 0.17	β = −0.30	β = −0.32	β = −0.16	β = 0.25*
	RD	R² = 0.16 p = 0.34	β = 0.24	β = −0.13	β = 0.17	β = 0.10	β = 0.24
	MD	R² = 0.35 p = 0.015	β = 0.23	β = −0.27	β = −0.15	β = −0.07	β = 0.29
	AWF	R² = 0.13 p = 0.47	β = −0.17	β = −0.08	β = 0.11	β = −0.15	β = −0.25
WMTI	Da	R² = 0.68 **p < 0.0001**	β = 0.09	β = −0.20	β = −0.31	β = −0.42***	β =0.10
	D_{Epar}	R² = 0.68 **p < 0.0001**	β = 0.13	β = −0.14	β = −0.45**	β = −0.32*	β = 0.14
	D_{Eperp}	R² = 0.14 p = 0.45	β = 0.20	β = −0.06	β = 0.00	β = −0.01	β = 0.27
Chronic Diffusion							
FP-DDE	ADC∥	R² = 0.51 **p = 0.0003**	β = 0.20	β = −0.36	β = −0.07	β = −0.28	β = 0.08
	f_R	R² = 0.37 p = 0.012	β = −0.25	β = 0.24	β = −0.10	β = 0.37	β = −0.03
DTI	FA	R² = 0.69 **p < 0.0001**	β = 0.11	β = −0.70***	β = −0.17	β = 0.08	β = −0.08
	AD	R² = 0.41 **p = 0.004**	β = 0.19	β = −0.60*	β = −0.13	β = −0.08	β = 0.07
	RD	R² = 0.47	β = −0.02	β = 0.51*	β = 0.27	β = −0.18	β = 0.16

		Mult. Reg.	SMI31	SMI32	ED1	DAPI	GFAP
		$p = 0.001$					
WMTI	MD	$R^2 = 0.15$ $p = 0.39$	$\beta = 0.09$	$\beta = 0.08$	$\beta = 0.31$	$\beta = -0.21$	$\beta = 0.18$
	AWF	$R^2 = 0.41$ $p = 0.004$	$\beta = -0.04$	$\beta = -0.45$	$\beta = -0.30$	$\beta = 0.18$	$\beta = -0.13$
	Da	$R^2 = 0.59$ $p < 0.0001$	$\beta = 0.02$	$\beta = -0.70^{***}$	$\beta = -0.15$	$\beta = 0.11$	$\beta = -0.03$
	D_{Epar}	$R^2 = 0.45$ $p = 0.002$	$\beta = 0.11$	$\beta = -0.56^{*}$	$\beta = -0.13$	$\beta = 0.03$	$\beta = 0.06$
	D_{Eperp}	$R^2 = 0.39$ $p = 0.008$	$\beta = -0.06$	$\beta = 0.33$	$\beta = 0.36$	$\beta = -0.16$	$\beta = 0.17$
BBB Scoring							
	Acute	$R^2 = 0.72$ $p < 0.0001$	$\beta = 0.20$	$\beta = -0.69^{***}$	$\beta = -0.07$	$\beta = -0.06$	$\beta = 0.00$
	Chronic	$R^2 = 0.63$ $p < 0.0001$	$\beta = 0.18$	$\beta = -0.67^{***}$	$\beta = -0.05$	$\beta = 0.03$	$\beta = 0.19$